Journal of Solid State Chemistry 182 (2009) 1245–1251

Contents lists available at ScienceDirect

Journal of Solid State Chemistry

journal homepage: www.elsevier.com/locate/jssc

Syntheses, crystal and electronic structures of three new potassium cadmium(II)/zinc(II) tellurides: $K_2Cd_2Te_3$, K_6CdTe_4 and K_2ZnTe_2

Min-Jie Li [a,b], Chun-Li Hu [a], Xiao-Wu Lei [a,b], Yong Zhou [a,b], Jiang-Gao Mao [a,*]

[a] State Key Laboratory of Structural Chemistry, Fujian Institute of Research on the Structure of Matter, Chinese Academy of Sciences, Fuzhou 350002, P.R. China
[b] Graduate School of the Chinese Academy of Sciences, Beijing 100039, P.R. China

ARTICLE INFO

Article history:
Received 25 December 2008
Received in revised form
11 February 2009
Accepted 15 February 2009
Available online 26 February 2009

Keywords:
Ternary tellurides
Solid-state syntheses
Crystal structures
Band structure calculations

ABSTRACT

Three new ternary potassium(I) zinc(II) or cadmium(II) tellurides, namely, $K_2Cd_2Te_3$, K_6CdTe_4 and K_2ZnTe_2, were synthesized by solid-state reactions of the mixture of pure elements of K, Cd (or Zn) and Te in Nb tubes at high temperature. $K_2Cd_2Te_3$ belongs to a new structure type and its structure contains a novel two-dimensional $[Cd_2Te_3]^{2-}$ layers perpendicular to the *b*-axis. K(5) cation is located at the center of five member rings of the 2D $[Cd_2Te_3]^{2-}$ layer, whereas other K^+ cations occupy the interlayer space. K_6CdTe_4 with a K_6HgS_4 type structure features a "zero-dimensional" structure composed of isolated $CdTe_4$ tetrahedra separated by the K^+ ions. K_2ZnTe_2 in the K_2ZnO_2 structural type displays 1D $[ZnTe_2]^{2-}$ anionic chains of edge sharing $[ZnTe_4]$ tetrahedra separated by the potassium(I) ions. $K_2Cd_2Te_3$, K_6CdTe_4 and K_2ZnTe_2 revealed a band gap of 1.93, 2.51 and 3.0 eV, respectively.

1. Introduction

The studies on metal chalcogenides have received lots of research attentions in recent years. This class of compounds may exhibit a variety of open-framework structures with good ion exchange properties [1–5]. Some of metal chalcogenides show excellent thermoelectric properties [6–8]. Furthermore metal chalcogenides are usually semiconductors and they can also form non-centrosymmetric structures with large second harmonic generation (SHG) response and excellent transmission properties in the mid-IR and far-IR region [9–11]. Compared with metal sulfides and selenides, tellurides are much less explored. We focus on the alkali-Zn/Cd–Te systems in order to explore new SHG materials used in the mid-IR and far-IR region. So far reports on this class of compounds are still very limited, the structurally characterized ternary phases include $K_2Cd_3Te_4$ (*Pnma*) [12], $Cs_2Cd_3Te_4$ (*Ibam*) and $Rb_2Cd_3Te_4$ (*C2/c*) [13]. In addition, a number of lanthanide(III)-containing quaternary phases such as $CsLnZnTe_3$ (Ln = La, Pr, Nd, Sm, Gd, Tb, Dy, Ho, Er, Tm, Y), $AYbZnTe$ (A = Rb, Cs) and $CsLnCdTe_3$ (Ln = La, Pr, Nd, Sm, Gd–Tm and Lu) have also been isolated by the Ibers group and the Wu group [14–16]. Our explorations on the ternary phases in K–Zn(Cd)–Te systems afforded three new compounds, namely, $K_2Cd_2Te_3$ with a new structural type, K_6CdTe_4 with a K_6HgS_4 type structure [17] and K_2ZnTe_2 with a K_2ZnO_2 type structure [18]. Herein we report their syntheses, crystal structures, band structures and optical properties.

2. Experimental

2.1. Materials and methods

All of chemicals were obtained from commercial sources and used without further purification. Microprobe elemental analyses on K, Zn, Cd and Te elements were performed on a field emission scanning electron microscope (FESEM, JSM6700F) equipped with an energy dispersive X-ray spectroscope (EDS, Oxford INCA). X-ray powder diffraction (XRD) patterns (Cu$K\alpha$) were collected on an XPERT-MPD θ–2θ diffractometer. Optical diffuse reflectance spectrum was measured at room temperature with a PE Lambda 900 UV–visible spectrophotometer. The instrument was equipped with an integrating sphere and controlled by a personal computer. $BaSO_4$ plate was used as a standard (100% reflectance). The absorption spectrum was calculated from reflectance spectrum using the Kubelka–Munk function: $\alpha/S = (1-R)^2/2R$ [19], where α is the absorption coefficient, S is the scattering coefficient which is practically wavelength-independent when the particle size is larger than 5 μm, and R is the reflectance.

2.2. Synthesis of $K_2Cd_2Te_3$

Due to the air sensitive nature of the three compounds, all synthetic operations were performed under an argon atmosphere

* Corresponding author. Fax: +86 591 83714946.
E-mail address: mjg@fjirsm.ac.cn (J.-G. Mao).

0022-4596/$ - see front matter © 2009 Elsevier Inc. All rights reserved.
doi:10.1016/j.jssc.2009.02.020

within a glove box. Red single crystals of $K_2Cd_2Te_3$ were initially obtained by the solid state reaction of a mixture of K (Alfa Aesar, 99.95%, bulk), Cd (Alfa Aesar, 99.95%, shot), Sn (Alfa Aesar, 99.5%, shot) and Te (Alfa Aesar, 99.99%, broken ingot) in a molar ratio of 1:1:1:2 in our attempt to synthesize a K–Cd–Sn–Te quaternary phase. The mixture was loaded into a niobium tube within an argon-filled glove box and then the Nb tube was arc-welded under an argon atmosphere. The Nb tube was subsequently sealed into an evacuated quartz tube ($\sim 10^{-4}$ Torr) and placed into a furnace. The sample was heated to 573 K in 6 h, kept at 573 K for 1 day, and then heated to 773 K in 6 h, kept at 773 K for 4 days, and then cooled to 473 K in 6 days at 2 K/h, before switching off the furnace. Microprobe elemental analyses on several single crystals indicate the absence of the Sn element and gave a molar ratio of K/Cd/Te of 2.1(2)/2.0(2)/3.2(2), which is very close to that from single-crystal structural analyses. After proper structural determination, a lot of efforts were tried to prepare the single phase product of $K_2Cd_2Te_3$, but were unsuccessful. The reaction of pure elements of K, Cd and Te in stoichiometric molar ratio gave $K_2Cd_3Te_4$ (*Pnma*) as the main product [12]. Changing reaction temperatures or starting materials (K_2Te and CdTe) also lead to $K_2Cd_3Te_4$ as the main product. The sample used for optical diffuse reflectance spectrum measurements are single crystals selected based on shape and color.

2.3. Syntheses of K_6CdTe_4 and K_2ZnTe_2

Single crystals of K_6CdTe_4 and K_2ZnTe_2 were initially prepared by reactions of a mixture of pure elements of K, Cd (or Zn) and Te in a molar ratio of 6:1:4 for K_6CdTe_4, or 2:1:2 for K_2ZnTe_2. The mixture was loaded into a niobium tube in an argon-filled glove box and then the Nb tube was arc-welded under an argon atmosphere. The Nb tube was subsequently sealed within an evacuated quartz tube ($\sim 10^{-4}$ Torr) and placed into the furnace. The samples were heated at 523 K for 1 day and then heated at 1023 (for K_6CdTe_4) or 973 K (for K_2ZnTe_2) for 1 day, and then cooled to 773 K at 2 K/h, kept at 773 K for 3 days, and then cooled to 473 K in 5 days at 2 K/h, before switching off the furnace. Results of EDS microprobe elemental analyses on several single crystals of K_6CdTe_4 and K_2ZnTe_2 gave a K/Cd(or Zn)/Te molar ratios of 6.1(2)/1.0(2)/4.2(2) and 2.2(2)/1.0(2)/2.2(2), respectively, for K_6CdTe_4 and K_2ZnTe_2. After structural analyses, the mono-phase products of K_6CdTe_4 and K_2ZnTe_2 were obtained quantitatively by the solid state reactions of a stoichiometric mixture of K/Cd (or Zn)/Te at 1023 (for K_6CdTe_4) or 973 K (for K_2ZnTe_2) for 5 days. Their purities were confirmed by XRD powder diffraction studies (see Supporting Materials).

2.4. Crystal structure determination

Data collections for $K_2Cd_2Te_3$, K_6CdTe_4 and K_2ZnTe_2 were performed on a Rigaku mercury CCD diffractometer equipped with a graphite-monochromated Mo*K*α radiation ($\lambda = 0.71073$ Å) at 293 K. The data sets were corrected for Lorentz and polarization factors as well as for absorption by multi-scan method [20]. All three structures were solved by the direct methods and refined by full-matrix least squares fitting on F^2 by SHELXTL 97 [21]. All atoms were refined with anisotropic thermal parameters. All of the atomic sites in the three compounds were fully occupied according to the site occupancy refinements. Final difference Fourier maps showed featureless residual peaks of 3.484 and -1.791 eÅ^{-3} (0.92 and 0.61 Å, respectively, away from Cd(6)) for $K_2Cd_2Te_3$, 0.779 and -1.304 eÅ^{-3} (0.96 and 1.05 Å from Te(1) and Cd(1), respectively) for K_6CdTe_4, 0.593 and -0.480 eÅ^{-3} (0.06 and 1.53 Å from Te(1) and K(1), respectively) for K_2ZnTe_2. Data collection and refinement parameters were summarized in Table 1, the atomic coordinates, important bond lengths and angles were listed in Tables 2 and 3 respectively.

Crystallographic data in CIF format for $K_2Cd_2Te_3$, K_6CdTe_4 and K_2ZnTe_2 have been given as Supporting Materials. These data can also be obtained from the Fachinformationszentrum Karlsruhe, 76344 Eggenstein-Leopoldshafen,

Table 1
Crystal data and structure refinement for $K_2Cd_2Te_3$, K_6CdTe_4 and K_2ZnTe_2.

Chemical formula	$K_2Cd_2Te_3$	K_6CdTe_4	K_2ZnTe_2
Formula weight	685.80	857.40	398.77
Crystal system	Monoclinic	Hexagonal	Orthorhombic
Space group	$P2_1/c$ (no. 14)	$P6_3mc$ (no. 186)	*Ibam* (no. 72)
a (Å)	13.259(3)	11.050(1)	7.303(3)
b (Å)	15.785(3)	11.050(1)	14.022(5)
c (Å)	14.266(3)	8.292(2)	6.921(2)
β (deg)	94.033(4)	90	90
V (Å^3)	2978.5(1)	876.9(2)	708.7(4)
Z	12	2	4
D_{calcd} (g/cm^3)	4.588	3.247	3.737
μ (Mo*K*α)/mm^{-1}	13.674	9.150	12.575
Reflections collected	22928	6203	2569
Unique reflections	6745	764	442
Reflections ($I>2\sigma(I)$)	5824	735	427
T (K)	293	293	293
GOF on F^2	1.078	1.190	1.049
$R1$, w$R2$ [$I>2\sigma(I)$][a]	0.0329, 0.0661	0.0294, 0.0655	0.0153, 0.0342
$R1$, w$R2$ (all data)	0.0407, 0.0701	0.0310, 0.0663	0.0165, 0.0346

[a] $R_1 = \sum||F_o|-|F_c||/\sum|F_o|$; $wR_2 = \sum w[(F_o)^2-(F_c)^2]^2/\sum w[(F_o)^2]^{21/2}$.

Table 2
Atomic coordinates and equivalent isotropic displacement parameters ($\times 10^3$ Å^2) for $K_2Cd_2Te_3$, K_6CdTe_4 and K_2ZnTe_2.

Atom	*Wyck*	*x*	*y*	*z*	*U* (eq)[a]
$K_2Cd_2Te_3$					
K1	4*e*	0.1424(2)	0.0379(2)	0.4399(2)	43(1)
K2	4*e*	0.3572(2)	0.0247(2)	0.0459(2)	35(1)
K3	4*e*	0.2486(2)	0.0295(2)	0.7328(1)	43(1)
K4	4*e*	0.4748(2)	0.0262(2)	0.3542(2)	46(1)
K5	4*e*	0.7351(2)	0.2706(2)	0.2324(2)	46(1)
K6	4*e*	0.0189(1)	0.0536(1)	0.1225(1)	48(1)
Cd1	4*e*	0.4429(1)	0.2306(1)	0.1808(1)	27(2)
Cd2	4*e*	0.6302(1)	0.2907(1)	0.4812(1)	30(2)
Cd3	4*e*	0.8621(1)	0.1917(1)	0.4905(1)	28(2)
Cd4	4*e*	0.1776(1)	0.2497(1)	0.0954(1)	27(2)
Cd5	4*e*	0.3189(1)	0.2535(1)	0.3863(1)	27(2)
Cd6	4*e*	0.9935(1)	0.2898(1)	0.3236(1)	34(2)
Te1	4*e*	0.5845(1)	0.1114(1)	0.1387(1)	24(2)
Te2	4*e*	0.2604(1)	0.1384(1)	0.2387(1)	23(2)
Te3	4*e*	0.1562(1)	0.1397(1)	0.9328(1)	24(1)
Te4	4*e*	0.4906(1)	0.3452(1)	0.3328(1)	24(2)
Te5	4*e*	0.0125(1)	0.3503(1)	0.1374(1)	27(2)
Te6	4*e*	0.8345(1)	0.3668(1)	0.4405(1)	26(2)
Te7	4*e*	0.9330(1)	0.1223(1)	0.3255(1)	31(2)
Te8	4*e*	0.6702(1)	0.3797(1)	0.0158(1)	33(2)
Te9	4*e*	0.3526(1)	0.3480(1)	0.0499(1)	23(2)
K_6CdTe_4					
K(1)	6*c*	0.4766(1)	0.9532(1)	0.9774(1)	38(1)
K(2)	6*c*	0.7021(1)	0.8510(1)	0.2912(1)	54(2)
Cd(1)	2*b*	1/3	2/3	0.5983(1)	24(1)
Te(1)	6*c*	0.6178(1)	0.8089(1)	0.7025(1)	24(1)
Te(2)	2*b*	1/3	2/3	0.2537(1)	34(1)
K_2ZnTe_2					
K(1)	8*j*	0.1799(1)	0.3579(1)	0	28(1)
Zn(1)	4*a*	0	0	1/4	19(1)
Te(1)	8*j*	0.1947(1)	0.1071(1)	0	20(1)

[a] *U* (eq) is defined as one-third of the trace of the orthogonalized U_{ij} tensor.

Table 3
Selected bond lengths (Å) and angles (deg) for $K_2Cd_2Te_3$, K_6CdTe_4 and K_2ZnTe_2.

$K_2Cd_2Te_3$					
K(1)–Te(2)	3.720(2)	K(2)–Te(1)	3.486(2)	K(3)–Te(1)	3.554(2)
K(1)–Te(5)	3.725(2)	K(2)–Te(1)	3.526(2)	K(3)–Te(3)	3.628(2)
K(1)–Te(5)	3.835(2)	K(2)–Te(2)	3.596(2)	K(3)–Te(4)	3.949(2)
K(1)–Te(7)	3.393(2)	K(2)–Te(3)	3.520(2)	K(3)–Te(5)	3.827(2)
K(1)–Te(8)	3.547(2)	K(2)–Te(4)	3.820(2)	K(3)–Te(7)	3.458(2)
K(1)–Te(9)	3.587(2)	K(2)–Te(6)	3.576(2)	K(3)–Te(9)	3.598(2)
K(4)–Te(1)	3.742(2)	K(5)–Te(1)	3.421(2)	K(6)–Te(2)	3.749(2)
K(4)–Te(2)	3.643(2)	K(5)–Te(4)	3.821(2)	K(6)–Te(3)	3.883(2)
K(4)–Te(4)	3.956(2)	K(5)–Te(6)	3.509(2)	K(6)–Te(3)	3.631(2)
K(4)–Te(8)	3.660(2)	K(5)–Te(7)	3.693(2)	K(6)–Te(6)	3.660(2)
K(4)–Te(8)	3.603(2)	K(5)–Te(8)	3.589(2)	K(6)–Te(6)	3.677(2)
K(4)–Te(9)	3.817(2)	K(4)–Te(9)	3.874(2)	K(6)–Te(7)	3.365(2)
Cd(1)–Te(1)	2.754(1)	Cd(2)–Te(1)	2.827(1)	Cd(3)–Te(5)	2.868(1)
Cd(1)–Te(2)	2.989(1)	Cd(2)–Te(4)	2.846(1)	Cd(3)–Te(6)	2.871(1)
Cd(1)–Te(4)	2.861(1)	Cd(2)–Te(6)	3.056(1)	Cd(3)–Te(7)	2.816(1)
Cd(1)–Te(9)	2.836(1)	Cd(2)–Te(8)	2.779(1)	Cd(3)–Te(8)	2.830(1)
Cd(4)–Te(2)	2.855(1)	Cd(5)–Te(2)	2.847(1)	Cd(6)–Te(3)	2.801(1)
Cd(4)–Te(3)	2.896(1)	Cd(5)–Te(3)	2.851(1)	Cd(6)–Te(5)	2.852(1)
Cd(4)–Te(5)	2.803(1)	Cd(5)–Te(4)	2.847(1)	Cd(6)–Te(6)	3.032(1)
Cd(4)–Te(9)	2.903(1)	Cd(5)–Te(9)	2.842(1)	Cd(6)–Te(7)	2.764(1)
Te(1)–Cd(1)–Te(9)	124.46(2)	Te(9)–Cd(1)–Te(2)	100.80(2)	Te(9)–Cd(1)–Te(4)	98.42(2)
Te(1)–Cd(1)–Te(4)	118.67(2)	Te(4)–Cd(1)–Te(2)	103.79(2)	Te(1)–Cd(1)–Te(2)	107.75(3)
Te(3)–Cd(6)–Te(6)	94.20(3)	Te(3)–Cd(6)–Te(5)	105.65(2)	Te(7)–Cd(6)–Te(3)	125.96(2)
Te(5)–Cd(6)–Te(6)	119.26(2)	Te(7)–Cd(6)–Te(6)	99.49(2)	Te(7)–Cd(6)–Te(5)	111.98(2)
K_6CdTe_4					
K(1)–Te(1)	3.559(2) × 2	K(1)–Te(2)	3.574(2)	K(2)–Te(1)	3.408(1) × 2
K(1)–Te(1)	3.772(2) × 2	K(2)–Te(1)	3.505(3)	Cd(1)–Te(1)	2.857(1) × 3
K(1)–Te(2)	4.083(2)	K(2)–Te(2)	3.544(3)	Cd(1)–Te(2)	2.858(2)
Te(1)–Cd(1)–Te(1)	111.27(2) × 3	Te(1)–Cd(1)–Te(2)	107.60(2) × 3		
K_2ZnTe_2					
K(1)–Te(1)	3.518(2)	K(1)–Te(1)	3.577(2)	K(1)–Te(1)	3.792(2)
K(1)–Te(1)	3.613(1) × 3	Zn(1)–Te(1)	2.6965(6) × 4		
Te(1)–Zn(1)–Te(1)	112.32(2) × 2	Te(1)–Zn(1)–Te(1)	116.34(2) × 2	Te(1)–Zn(1)–Te(1)	100.17(2) × 2

Germany (fax: +49 7247 808 666; e-mail: crysdata@fiz-karlsruhe.de) on quoting the depository numbers CSD 420089, 420087 and 420088.

2.5. Electronic structure calculations

Single-crystal structural data of $K_2Cd_2Te_3$, K_6CdTe_4 and K_2ZnTe_2 were used for theoretical calculations. Band structures and density of states (DOS) calculations were performed with the total energy code CASTEP [22–24]. The total energy was calculated by using density functional theory (DFT) by employing the Perdew–Burke–Ernzerh of generalized gradient approximation [25]. The interactions between the ionic cores and the electrons were described by the ultrasoft pseudopotential [26,27]. The following orbital electrons were treated as valence: Cd-$4d^{10}5s^2$, Zn-$3d^{10}4s^2$, Te-$5s^25p^4$ and K-$3s^23p^64s^1$. Considering the balance of computational cost and precision, we choose a cutoff energy of 260, 260 and 310 eV, respectively for $K_2Cd_2Te_3$, K_6CdTe_4 and K_2ZnTe_2. The other calculation parameters and convergent criteria were the default values of the CASTEP code.

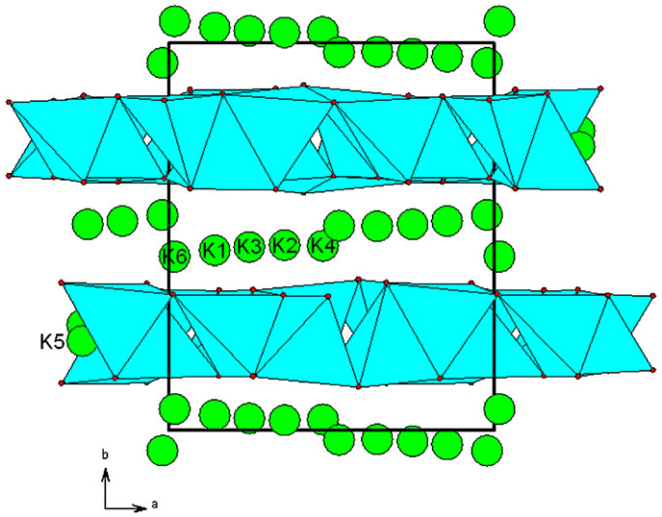

Fig. 1. View of the structure of $K_2Cd_2Te_3$ down the *c*-axis. $CdTe_4$ tetrahedra are shaded in cyan. K atoms are drawn as green circles. (For interpretation of the references to color in the figure legend, the reader is referred to the web version of this article.)

3. Results and discussions

Three new ternary potassium cadmium (or zinc) tellurides, namely, $K_2Cd_2Te_3$, K_6CdTe_4 and K_2ZnTe_2 had been successfully prepared by high-temperature solid-state reactions. Their structures feature 2D, 1D and 0D anionic units that are separated by potassium(I) cations.

$K_2Cd_2Te_3$ belongs to a new structure type and exhibits novel 2D $[Cd_2Te_3]^{2-}$ layers perpendicular to the *b*-axis that are separated by K+ ions (Fig. 1). There are six K, six Cd and nine Te atoms in the asymmetric unit of $K_2Cd_2Te_3$. All of six Cd(II) ions are tetrahedrally coordinated by four Te atoms. The Cd–Te distance

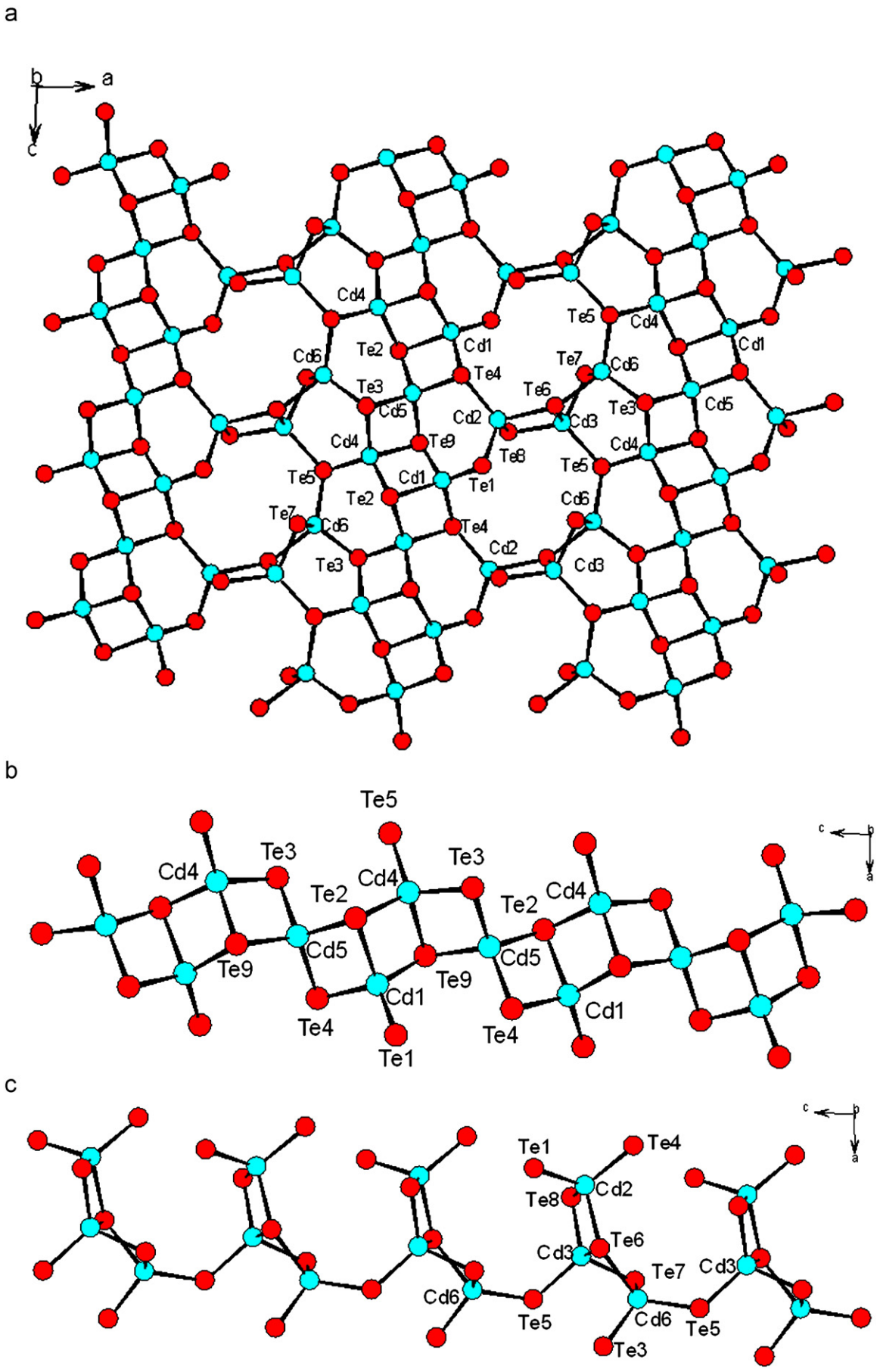

Fig. 2. A 2D layer $[Cd_2Te_3]^{2-}$ layer (a), a 1D Cd(1,4,5)–Te chain (b) and a 1D Cd(2,3,6)–Te chain (c) in $K_2Cd_2Te_3$.

range from 2.754(1) to 3.056(1) Å, and Te–Cd–Te bond angles are in the range of 94.20(3)°–125.96(2)°; hence, the $CdTe_4$ tetrahedra are significantly distorted (Table 3). These bond distances and angles are comparable to those reported in $K_2Cd_3Te_4$ [12].

The interconnection of $CdTe_4$ tetrahedra via edge- and corner-sharing resulted in a novel anionic layer of $[Cd_2Te_3]^{2-}$(Fig. 2a). $Cd(1)Te_4$, $Cd(3)Te_4$ and $Cd(4)Te_4$ each shares two edges and one corner with three neighbors, $Cd(5)Te_4$ shares two edges with two other Cd(II) ions, whereas $Cd(2)Te_4$ and $Cd(6)Te_4$ each shares one edge and two corners with three Cd(II) ions. The two-dimensional $[Cd_2Te_3]^{2-}$ layer in $K_2Cd_2Te_3$ can be described as formed by two types of 1D chains along *c* axis: one formed by $Cd(1)Te_4$, $Cd(4)Te_4$ and $Cd(5)Te_4$ interconnected via edge-sharing (Fig. 2b), and the other formed by trimers of edge-sharing $Cd(2)Te_4$, $Cd(3)Te_4$ and $Cd(6)Te_4$, these trimers are further interconnected via corner sharing Te(5) corners (Fig. 2c). The above two types of chains are alternating along *a*-axis and interconnected via Cd–Te–Cd bridges, forming five-member polyhedral rings (Fig. 2a).

It should be noted that the 2D $[Cd_2Te_3]^{2-}$ layer in $K_2Cd_2Te_3$ differs significantly from the $[Cd_3Te_4]^{2-}$ layer in $K_2Cd_3Te_4$ [12]. The $[Cd_3Te_4]^{2-}$ layer in $K_2Cd_3Te_4$ is based on $[Cd_3Te_4]^{2-}$ clusters which can be viewed as truncated cubes [12].

K(1), K(2), K(3), K(4) and K(6) ions occupy the interlayer space whereas K(5) atoms are located at the centers of the five-member rings of the 2D $[Cd_2Te_3]^{2-}$ layer. The interlayer distance of about 7.9 Å is slightly larger than that in $K_2Cd_3Te_4$ (7.57 Å) [12]. All six K^+ ions are octahedrally coordinated by six Te atoms with K–Te distances in the range of 3.365(2)–3.956(2) Å, hence these octahedra are severely distorted.

The structure of K_6CdTe_4 features isolated $[CdTe_4]$ tetrahedra which are separated by the K^+ ions, as shown in Fig. 3. It is isostructural with K_6HgS_4 [17], hence only a brief structure description is provided. There are two K, one Cd and two Te atoms in the asymmetric unit of K_6CdTe_4. Cd(1) and Te(2) lie on sites of 3*m* symmetry whereas the other atoms occupy the general positions. The Cd(II) ion is tetrahedrally coordinated by four Te atoms with Cd–Te distances in the range of 2.857(1)–2.858(2) Å. The Te–Cd–Te bond angles are 111.27(3)° and 107.60(2)°, respectively. Hence, the $CdTe_4$ tetrahedron is only slightly distorted. K(1) is six-coordinated by six Te atoms with K–Te distances in the range of 3.559(2)–4.083(2) Å, whereas K(2) is tetrahedrally coordinated by four Te atoms with K–Te distances ranging from 3.408(1) to 3.544(3) Å (see supporting materials and Table 3). We deem that the lower dimension of structure of K_6CdTe_4 is due to smaller Cd/Te ratio (1:4) than compared with that of $K_2Cd_2Te_3$ (2:3); hence, no edge or corner-sharing of $CdTe_4$ tetrahedra is necessary.

K_2ZnTe_2 is the first compound in alkali metals–*M*–Te (*M* = Zn, Cd, Hg) systems with a 1D anionic structure. It features 1D infinite $[ZnTe_2]^{2-}$ chains along the *c*-axis composed of edge-sharing $[ZnTe_4]$ tetrahedra separated by K^+ ions (Fig. 4). It is isostructural with K_2ZnO_2 [18]. The Zn–Te distances are 2.6965(6) Å and Te–Zn–Te bond angles range from 100.17(2)° to 116.34(2)°, which are comparable to those reported in 1D $(N_2H_4)_2ZnTe$ [28]. The K^+ ion is surrounded by six Te atoms with K–Te distances of 3.518(2)–3.792(2) Å (See Supporting Materials and Table 3). The Zn/Te ratio of 1:2 is in-between Cd/Te ratios of 2:3 in $K_2Cd_2Te_3$ and 1:4 in K_6CdTe_4; hence, $[ZnTe_2]^{2-}$ anion exhibit a 1D chain structure. Clearly the Zn(Cd)/Te ratio has a strong effect on the dimension of the anion formed.

3.1. Absorbance spectrum

Optical reflectance spectrum measurements indicate that the band gaps of $K_2Cd_2Te_3$, K_6CdTe_4 and K_2ZnTe_2 are approximately 1.93, 2.51 and 3.0 eV (Fig. 5). Hence, all of them are semiconductors, which is in agreement with the dark red, dark yellow and pale yellow colors of $K_2Cd_2Te_3$, K_6CdTe_4 and K_2ZnTe_2. These band-gap energies are also comparable to the values of other compounds in the *A*–Cd(Zn)–Te (*A* = alkali metals) family (2.48 eV

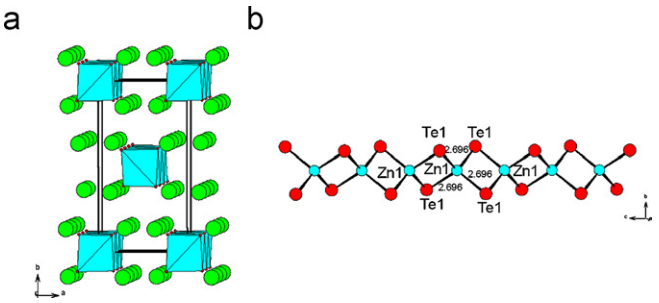

Fig. 4. View of the structure of K_2ZnTe_2 down the *c*-axis (a) and a 1D zinic telluride chain along *c*-axis (b). $ZnTe_4$ tetrahedra are shaded in cyan and K atoms are drawn as green circles. (For interpretation of the references to color in the figure legend, the reader is referred to the web version of this article.)

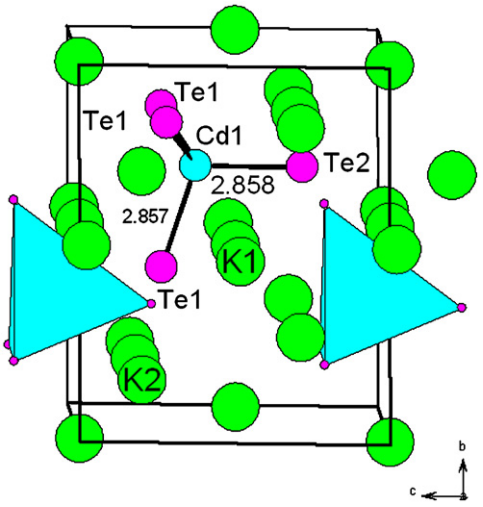

Fig. 3. View of the structure of K_6CdTe_4 down the *a*-axis. $CdTe_4$ tetrahedra are shaded in cyan. K, Cd and Te atoms are drawn as green, cyan and pink circles, respectively. (For interpretation of the references to color in the figure legend, the reader is referred to the web version of this article.)

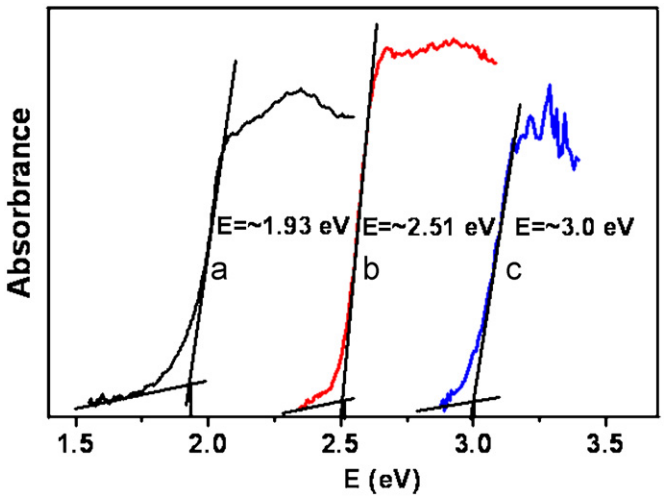

Fig. 5. Optical diffuse reflectance spectra for (a) $K_2Cd_2Te_3$, (b) K_6CdTe_4 and (c) K_2ZnTe_2.

for $Cs_2Cd_3Te_4$, 2.30 eV for $Rb_2Cd_3Te_4$, and 2.26 eV for $K_2Cd_3Te_4$) [12,13].

3.2. Theoretical studies

To further understand the chemical bonding and electronic structures of $K_2Cd_2Te_3$, K_6CdTe_4 and K_2ZnTe_2, band structures as well as DOS calculations based on the DFT method were performed by using the computer code CASTEP.

The calculated band structures of $K_2Cd_2Te_3$, K_6CdTe_4 and K_2ZnTe_2 along high-symmetry points within the first Brillouin zones are plotted in Fig. 6. It is found that the top of valence bands (VBs) is almost flat, whereas the bottom of conduction bands (CBs) displays some dispersion for $K_2Cd_2Te_3$ and K_6CdTe_4. The top of VBs and bottom of CBs are both flat for K_2ZnTe_2. For $K_2Cd_2Te_3$, K_6CdTe_4 and K_2ZnTe_2, the lowest energy of the CBs (1.52, 1.86 and 2.30 eV) are all at G point, whereas the highest energy (0.0 eV) of their VBs are also located at G point. Therefore, $K_2Cd_2Te_3$, K_6CdTe_4 and K_2ZnTe_2 display direct band gaps of 1.52, 1.86 and 2.30 eV, respectively. These values are slightly smaller than the experimental ones. Such discrepancy is due to the limitation of DFT method that sometimes underestimates the band gap in semiconductors and insulators [29–33].

The density-of-states (DOS) of the three compounds have been calculated to understand the distribution of valence orbitals of each atom near the Fermi level. The bands can be assigned according to the total and partial densities of states (DOS) as plotted in Fig. 7. For $K_2Cd_2Te_3$, the regions below the Fermi level (the Fermi level is set at 0 eV) can be divided into three regions. The VBs ranging from −35.0 to −12.5 eV are mainly formed by the states of K-3*s* and K-3*p* states. The VBs ranging from −12.5 to −5.0 eV are mainly composed of Cd-4*d* and Te-5*s* states. The sharp peak of Cd-4*d* orbital at around −8 eV indicates that the Cd-4*d* electrons are highly localized. The main contributions of VBs ranging from −5 eV to the Fermi level (0.0 eV) are mainly Cd-5*p*, Cd-5*s* and Te-5*p* states. As shown in Fig. 7a, it is observed that the densities of Te-5*p* states are larger than those of Cd-5*s*, Cd-5*p* between −2.5 eV and the Fermi level, indicating that the hybridization of Cd-5*s*, Cd-5*p* with Te-5*p* states and the covalent bonding between Cd and Te atoms. The bands just above the Fermi level are derived from Cd-5*s*, Te-5*s*, and Te-5*p* states whereas the VBs just below the Fermi level are mainly of Te-5*p* and Cd-5*p* states. Therefore, the optical absorptions can mainly be ascribed to the charge transitions from Te-5*p* to Cd-5*s* states.

The TDOS and PDOS of K_6CdTe_4 and K_2ZnTe_2 exhibit many similarities to those of $K_2Cd_2Te_3$. The bands just above the Fermi level are derived from K-3*p* states mixed with small amount of Cd-5*s* and Te-5*s* states for K_6CdTe_4. The VBs just below the Fermi level are mainly from Te-5*p*, K-4*s* and K-3*p* states for K_6CdTe_4. Therefore, the optical absorptions in K_6CdTe_4 can mainly be ascribed to the charge transitions from Te-5*p* to K-4*s* and K-3*p* states. For K_2ZnTe_2, the PDOS in the range of −5 to 7.5 eV is essentially same as K_6CdTe_4 except that the bands just above the Fermi level are derived from Zn-4*s* states mixed with small amount of K-3*p* and Te-5*p* states. Therefore, the optical absorptions in K_2ZnTe_2 can mainly be ascribed to the charge transitions from Te-5*p* to Zn-4*s* states.

Semi-empirical population analyses allow for a more quantitative bond analysis. The calculated bond orders of Cd–Te and K–Te bonds are −0.13–0.59e, −0.18–0.71e (covalent single-bond order is generally 1.0e), respectively, for $K_2Cd_2Te_3$. The bond orders of Cd–Te and K-Te bonds in K_6CdTe_4 are 0.72–1.03e, −0.39–1.28e, respectively. The bond orders of Zn–Te and K–Te bonds are 0.15e, −0.59–1.53e, respectively, for K_2ZnTe_2. Hence, Cd(Zn)–Te bonds are significantly covalent in character, whereas

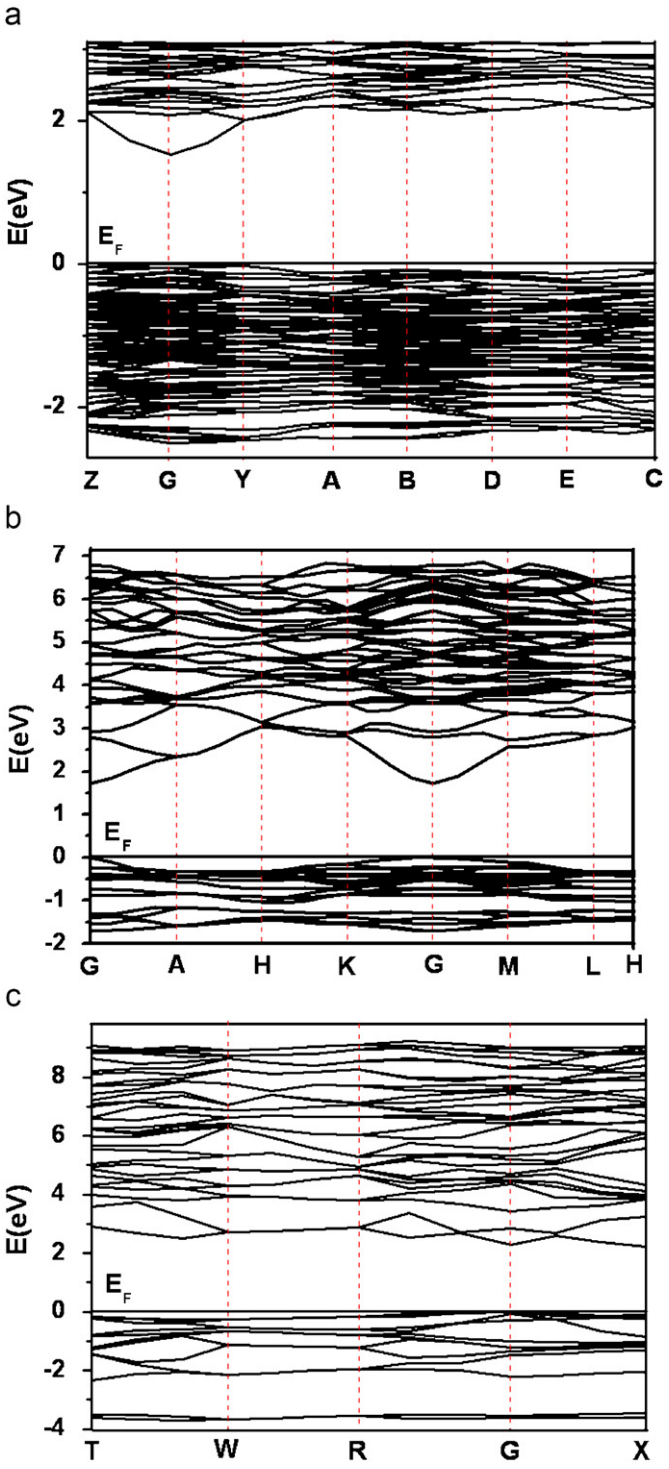

Fig. 6. Band structures of (a) $K_2Cd_2Te_3$, in the range of −2.7 and 3.1 eV, (b) K_6CdTe_4, in the range of −2 and 7 eV and (c) K_2ZnTe_2, in the range of −4 and 9.8 eV. The Fermi level is set at 0 eV.

the K–Te bonds are essentially ionic in character. It is also found that the Cd–Te bonding interactions in K_6CdTe_4 are much stronger than those in $K_2Cd_2Te_3$ and Zn–Te bonds in K_2ZnTe_2.

4. Conclusion

In conclusion, the syntheses, crystal and band structures as well as optical properties of $K_2Cd_2Te_3$, K_6CdTe_4 and K_2ZnTe_2 have

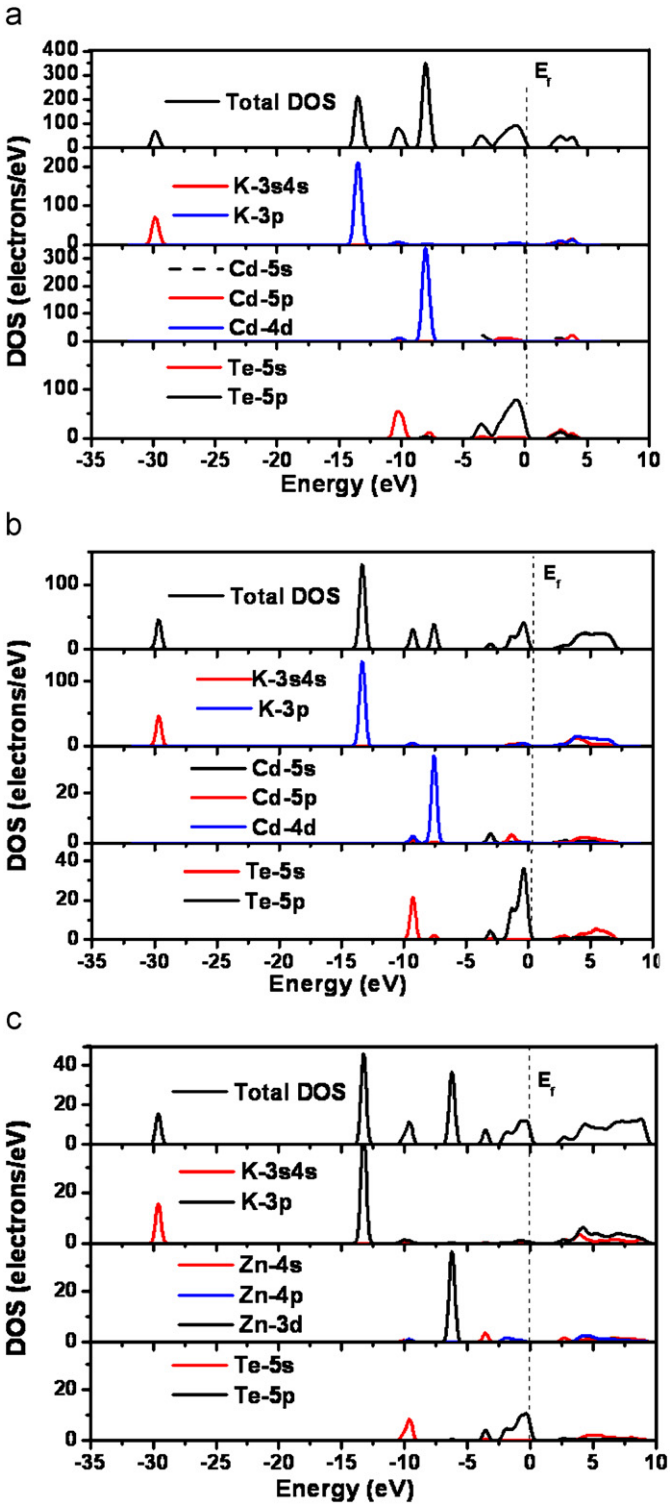

Fig. 7. Total and partial DOS of (a) $K_2Cd_2Te_3$, (b) K_6CdTe_4 and (c) K_2ZnTe_2. The Fermi level is set at 0 eV.

been described. $K_2Cd_2Te_3$ exhibits a novel two-dimensional anionic $[Cd_2Te_3]^{2-}$ layers. K_6CdTe_4 with a "zero-dimensional" structure contains isolated $CdTe_4$ tetrahedra. K_2ZnTe_2 features 1D $[ZnTe_2]^{2-}$ chains formed by edge sharing $[ZnTe_4]$ tetrahedra. It is found that the Cd/(or Zn)/Te ratio has a strong effect on the dimension of the anionic units formed. The cationic size is also important as exampled by the fact that $A_2Cd_3Te_4$ (A = K, Rb, Cs) formed three types of layered structures. These compounds are usually semiconductors. Our future research efforts will be focused on the syntheses, crystal structures as well as optical properties of other compounds in the A–Zn(Cd)–Te systems.

Acknowledgments

The authors gratefully acknowledge the financial support from the National Nature Science Foundation of China (nos. 20825104, 20573113, 20731006 and 20821061).

Appendix A. Supplementary material

Supplementary data associated with this article can be found in the online version at 10.1016/j.jssc.2009.02.020.

References

[1] M.J. Manos, K. Chrissafis, M.G. Kanatzidis, J. Am. Chem. Soc. 128 (2006) 8875–8883.
[2] N. Ding, M.G. Kanatzidis, Angew. Chem. Int. Ed. 45 (2006) 1397–1401.
[3] M.J. Manos, R.G. Iyer, E. Quarez, J.H. Liao, M.G. Kanatzidis, Angew. Chem. Int. Ed. 44 (2005) 3552–3555.
[4] M.J. Manos, C.D. Malliakas, M.G. Kanatzidis, Chem. Eur. J. 13 (2007) 51–58.
[5] N. Ding, D.-Y. Chung, M.G. Kanatzidis, Chem. Commun. (2004) 1170–1171.
[6] I.U. Arachchige, J.S. Wu, V.P. Dravid, M.G. Kanatzidis, Adv. Mater. 20 (2008) 3638.
[7] J.R. Sootsman, H. Kong, C. Uher, J.J. D'Angelo, C.I. Wu, I.P. Hogan, T. Caillat, M.G. Kanatzidis, Angew. Chem. In. Ed. 47 (2008) 8618–8622.
[8] J.H. Kim, D.Y. Chung, M.G. Kanatzidis, Chem. Commun. (2006) 1628–1630.
[9] S. Banerjee, C.D. Malliakas, J.I. Jang, J.B. Ketterson, M.G. Kanatzidis, J. Am. Chem. Soc. 130 (2008) 12270–12272.
[10] M.J. Manos, J.I. Jang, J.B. Ketterson, M.G. Kanatzidis, Chem. Commun. (2008) 972–974.
[11] I. Chung, J.I. Jang, M.A. Gave, D.P. Weliky, M.G. Kanatzidis, Chem. Commun. (2007) 4998–5000.
[12] E.A. Axtell III, J.-H. Liao, Z. Pikramenou, M.G. Kanatzidis, Chem. Eur. J. 2 (1996) 656–666.
[13] A.A. Narducci, J.A. Ibers, J. Alloys Compds. 306 (2000) 170–174.
[14] K. Mitchell, F.Q. Huang, E.N. Caspi, A.D. McFarland, C.L. Haynes, R.C. Somers, J.D. Jorgensen, R.P. Van Duyne, J.A. Ibers, Inorg. Chem. 43 (2004) 1082–1089.
[15] J. Yao, B. Deng, L.J. Sherry, A.D. McFarland, D.E. Ellis, R.P. Van Duyne, J.A. Ibers, Inorg. Chem. 43 (2004) 7735–7740.
[16] Y. Liu, L. Chen, L.M. Wu, G.H. Chan, R.P. Van Duyne, Inorg. Chem. 47 (2008) 855–862.
[17] H. Sommer, R. Hoppe, M. Jansen, Naturwissenschaften 63 (1976) 194–195.
[18] E. Vielhaber, R. Hoppe, Z. Anorg. Allg. Chem. 360 (1968) 7–14.
[19] W.M. Wendlandt, H.G. Hecht, Reflectance Spectroscopy, Interscience, New York, 1966.
[20] CrystalClear Version 1.3.5., Rigaku Corporation, Woodlands, TX, USA, 1999.
[21] G.M. Sheldrick, SHELXTL, Crystallographic Software Package, SHELXTL, Version 5.1, Bruker-AXS, Madison, WI, 1998.
[22] M.D. Segall, P.L.D. Lindan, M.J. Probert, C.J. Pickard, P.J. Hasnip, S.J. Clark, M.C. Payne, J. Phys.: Condens. Matter 14 (2002) 2717–2744.
[23] V. Milman, B. Winkler, J.A. White, C.J. Pickard, M.C. Payne, E.V. Akhmatskaya, R.H. Nobes, Int. J. Quant. Chem. 77 (2000) 895–910.
[24] M. Segall, P. Linda, M. Probert, C. Pickard, P. Hasnip, S. Clark, M. Payne, Materials Studio CASTEP, Version 2.2, 2002.
[25] J.P. Perdew, K. Burke, M. Ernzerhof, Phys. Rev. Lett. 77 (1996) 3865–3868.
[26] J.S. Lin, A. Qteish, M.C. Payne, V. Heine, Phys. Rev. B 47 (1993) 4174–4180.
[27] D.R. Hamann, M. Schluter, C. Chiang, Phys. Rev. Lett. 43 (1979) 1494–1497.
[28] D.B. Mitzi, Inorg. Chem. 44 (2005) 7078–7086.
[29] B. Deng, G.H. Chan, F.Q. Huang, D.L. Gray, D.E. Ellis, R.P. Van Duyne, J.A. Ibers, J. Solid State Chem. 180 (2007) 759–764.
[30] H.-L. Jiang, F. Kong, J.-G. Mao, J. Solid State Chem. 180 (2007) 1764–1769.
[31] R.W. Godby, M. Schluther, L.J. Sham, Phys. Rev. B 36 (1987) 6497–6500.
[32] C.M.I. Okoye, J. Phys.: Condens. Matter 15 (2003) 5945–5958.
[33] H.-L. Jiang, J.-G. Mao, J. Solid State Chem. 181 (2008) 345–354.